Imaging charge migration in the asymmetric molecule with the holographic interference in strong-field tunneling ionization

To cite this article: Mingrui He *et al* 2018 *J. Phys. B: At. Mol. Opt. Phys.* **51** 245602

View the article online for updates and enhancements.

IOP ebooks™

Bringing you innovative digital publishing with leading voices to create your essential collection of books in STEM research.

Start exploring the collection - download the first chapter of every title for free.

Imaging charge migration in the asymmetric molecule with the holographic interference in strong-field tunneling ionization

Mingrui He[1] , **Yueming Zhou**[1], **Jia Tan**[1], **Yang Li**[1], **Min Li**[1] and **Peixiang Lu**[1,2]

[1] School of Physics and Wuhan National Laboratory for Optoelectronics, Huazhong University of Science and Technology, Wuhan 430074, People's Republic of China
[2] Laboratory of Optical Information Technology, Wuhan Institute of Technology, Wuhan 430205, People's Republic of China

E-mail: zhouymhust@hust.edu.cn and lupeixiang@hust.edu.cn

Abstract

Coherent superposition of several electronic states in molecules induces attosecond charge migration. We theoretically demonstrate a way to observe this attosecond charge migration in the asymmetric molecule HeH^{2+} using strong-field photoelectron holography, complementary to our previous work (He M *et al* 2018 *Phys. Rev. Lett.* **120**, 133204) where the charge migration in the symmetric molecule was monitored. We disentangle the holographic interference from other types of interference in the photoelectron momentum distribution with the Fourier frequency filter method. By employing the holographic fringes originating from the ground state of HeH^{2+} as a reference, we develop a feasible approach to visualize the charge migration in the asymmetric molecule with attosecond temporal resolution.

Keywords: above-threshold ionization, strong laser field, ultrafast phenomena

(Some figures may appear in colour only in the online journal)

1. Introduction

The dynamics of the valence electron inside a single molecule plays a fundamental role in many biological processes and chemical reactions, unfolding on attosecond to femtosecond time scales [1–3]. In the past decades, charge migration in molecules originating from the valence electron photoionization or excitation has drawn much attention [4–8]. When an electron is suddenly removed from the neutral molecule, the residual will be in a superposition of various electronic states [9, 10]. The evolution of this coherent superposition state is labeled as charge migration to be distinguished from the charge transfer, where nuclear dynamics plays a dominant role [11]. The natural time scale of the charge migration ranges from hundreds of attoseconds to a few femtoseconds, depending on the composition of the superposed electron wave packet (EWP) and the conformation of the molecule [9, 12]. The rapidly developing attosecond technology [13–17, 42–44] has facilitated the

measurement with unprecedented temporal resolution, which opens up the way for tracing the ultrafast charge migration in molecules. By applying an isolated attosecond pulse, one can initiate charge migration in the molecule and then, observe it with another probe pulse [1, 2]. In previous studies, several attosecond methodologies also have been used to observe the charge migration, including attosecond transient absorption [18, 19], high-order harmonic spectroscopy [20–22], attosecond streaking [23], etc. Complementary to these measurements, recollision-based strong-field photoelectron holography (SFPH) is highly expected to access the valence electron motion on its intrinsic time scale [24, 25]. Recently, we have theoretically demonstrated the SFPH based method to visualize the attosecond charge migration in the symmetric molecule [26]. In that scheme, the imprint of the valence electron dynamics has been extracted from the recollision-based holographic pattern with a simple differential algorithm. However, this differential algorithm is not applicable when it comes to asymmetric molecules.

The recollision-based photoelectron holographic interference originates from the interference between the EWPs that re-collide with the parent ion and that reach the detector directly after tunneling ionization in the laser field [14, 27, 28]. Usually, in the photoelectron momentum distribution (PEMD), this SFPH pattern is mixed with other interference patterns, such as the intracycle interference that arises from the direct EWPs released in one laser cycle [29–31]. Therefore, it is necessary to disentangle certain interference pattern from the PEMD [32–34] before extracting information from it. In this study, we numerically solve the time-dependent Schrödinger equation (TDSE) to investigate the tunneling ionization of both the ground state and the coherent superposition state of HeH^{2+}. Various interference patterns appear in the obtained PEMDs. We propose the Fourier frequency filter method to separate the recollision-based SFPH pattern from the PEMD. With this procedure, the holographic interference is successfully separated from other types of interference. For the asymmetric molecule, the previously demonstrated procedure [26] to extract the electronic dynamical information from the holographic fringes is not applicable. In this study, by employing the holographic fringes of the ground state as a reference, we achieve the visualization of the ultrafast charge migration in HeH^{2+}. This work will encourage further attempt to extend our SFPH method to monitor the electronic dynamics in more complicated molecules.

2. Theory and results

We use the prototypical molecular ion HeH^{2+} aligned perpendicular to the laser polarization direction to investigate the charge migration in asymmetric molecule. Considering a coherent superposition state composed by two electronic states (atomic units are used unless otherwise stated)

$$\Psi(\vec{r}, t) = c_g \Psi_g(\vec{r}) e^{-iE_g t} + c_e \Psi_e(\vec{r}) e^{-i(E_e t + \theta_0)}, \quad (1)$$

where $\Psi_{g,e}$ are the ground state ($1s\sigma_g$) and the first excited state ($2p\sigma_u$) of HeH^{2+} with eigen-energies E_g and E_e, respectively. c_g and c_e are the corresponding expansion coefficients of the two states ($c_g^2 + c_e^2 = 1$). θ_0 denotes the initial relative phase. Experimentally, this superposition state can be prepared by the excitation of the ground state with an attosecond pump pulse [4, 10], and θ_0 is adjustable by changing the pump-probe delay. We mention that in the real experiment, θ_0 will have a distribution, and thus decrease the coherence of the superposition state.

The ionization of this superposition state in the laser field is studied by numerically solving the two-dimensional (2D) TDSE (in plane coordinate (x, y)) with a static nucleus frame in the length gauge, which can be written as

$$i \frac{\partial}{\partial t} \Psi(\vec{r}, t) = \left[-\frac{1}{2}\nabla^2 + V(r) + \vec{r} \cdot \vec{E}(t) \right] \Psi(\vec{r}, t). \quad (2)$$

Here, we adopt a two-center soft-core molecular potential $V(x, y) = -2/\sqrt{x^2 + (y - R/2)^2 + \eta} - 1/\sqrt{x^2 + (y + R/2)^2 + \eta}$ to mimic HeH^{2+} aligned along the y-axis with internuclear separation $R = 6$ a.u. In our simulation, the soft-core
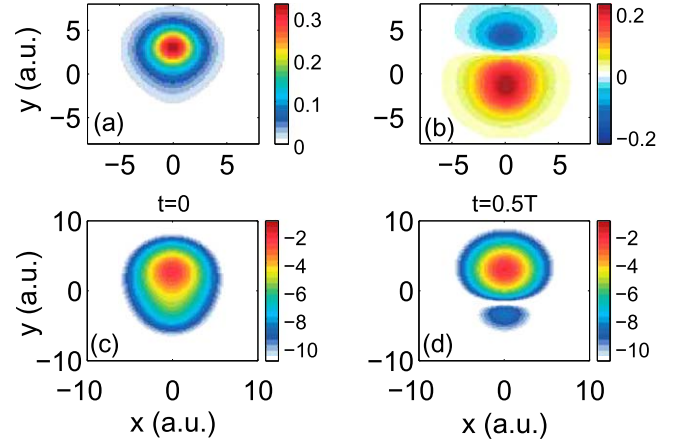

Figure 1. (a) The electron wave function of the ground state of HeH^{2+} in coordination space. (b) Same as (a), but for the first excited state of HeH^{2+}. (c) The moduli of the superposition state composed by the states in (a) and (b) with relative coefficient $c_g^2 : c_e^2 = 32:1$ and initial phase $\theta_0 = 0$ at the instant $t = 0$. (d) Same as (c), but for the instant $t = 0.5T$ (T is the oscillation period of the superposition state).

parameter η is set to be 3, producing the energies of the bound states $E_g = -0.88$ a.u. and $E_e = -0.66$ a.u.. Therefore, the oscillation period of the superposition state $\Psi(\vec{r}, t)$ reads $T = 2\pi/\Delta E = 28.5$ a.u. $\vec{E}(t)$ is the electric field of a linearly polarized (along x-axis) single-cycle model laser pulse [35] defined as $\vec{E}(t) = -\sqrt{(2e)}E_0(2t/\tau)e^{-(2t/\tau)^2}$ with the amplitude $E_0 = 0.0826$ (corresponding to the intensity of 2.4×10^{14} W cm^{-2}) and the duration $\tau = 170$ (laser wavelength $\lambda \approx 1800$ nm). This 2D TDSE is solved by using the split-operator spectral method [36] on a Cartesian grid ranges from -400 to 400 a.u. The time step is fixed at $\Delta t = 0.1$ a.u. and the spatial discretization is $\Delta x = \Delta y = 0.2$ a.u.

Figures 1(a) and (b) present the electron wave functions of the ground state ($1s\sigma_g$) and the first excited state ($2p\sigma_u$) of HeH^{2+}, respectively. The electron wave function is concentrated on He^{2+} ion for the $1s\sigma_g$ state due to the asymmetric nuclear charge [37] and it has a larger portion on H$^+$ for the $2p\sigma_u$ state. For the superposition state composed by these two states, the EWP oscillates in the molecule, as shown in figures 1(c) and (d) where we display the electron density distribution at two instants of $t = 0$ and $0.5T$. Here the relative coefficients $c_g^2 : c_e^2 = 32:1$ and the initial relative phase $\theta_0 = 0$. We use this coefficients ratio as an example to illustrate our scheme, which is not restrict to a specific ratio. Figure 2 presents the PEMDs for the tunneling ionization of the ground state and the superposition state of HeH^{2+} by the same laser field (with parameters described above). Figures 2(a)–(c) show the results for ionization from the ground state and superposition state with $\theta_0 = 0$ and $\pi/2$, respectively. In the PEMDs, the nearly vertical interference fringes originate from the intracycle interference, and the nearly horizontal ones are the recollision-based holographic stripes. Note that for the symmetric molecule [26], the recollision-based SFPH pattern of the ground state is exactly symmetric about $p_y = 0$. But for the asymmetric molecule HeH^{2+}, these holographic fringes for both the ground state
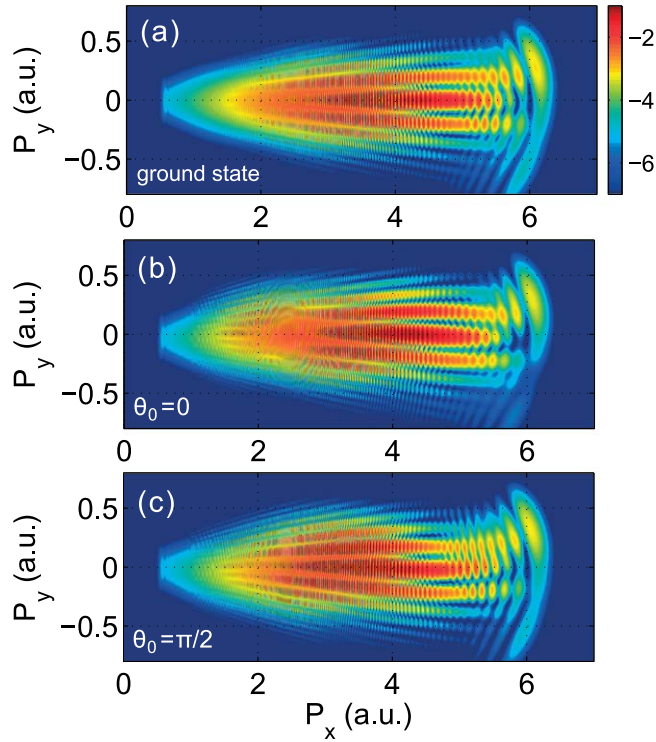
J. Phys. B: At. Mol. Opt. Phys. **51** (2018) 245602

M He *et al*

Figure 2. (a) The photoelectron momentum distribution (PEMD) of the ground state of HeH^{2+} tunneling ionized by a single-cycle laser field with the wavelength of 1800 nm and intensity of 2.4×10^{14} W cm^{-2}. (b) And (c) same as (a), but for tunneling ionization of the superposition state of HeH^{2+} with relative coefficient $c_g^2 : c_e^2 = 32:1$ and initial relative phase $\theta_0 = 0$ and $\pi/2$, respectively.

and the superposition state are asymmetric about $p_y = 0$. We notice that in previous work [38], this asymmetric holographic interference for the ground state of HeH^{2+} can be observed, which is faint because the internuclear separation used in that calculation is small. In what follows, we will explain the formation of the asymmetric recollision-based holographic patterns and demonstrate how to extract the electronic dynamical information from them.

The recollision-based SFPH pattern originates from the interference between EWPs that reach the detector directly (direct electron) and that re-collide with the parent ion (rescattered electron). This kind of interference is determined by the phase difference between the direct and the rescattered electrons, which reads [26]

$$\Delta\varphi(p_y) = \tfrac{1}{2}p_y^2(t_r - t_i) + \alpha + [\phi(0; t_i) - \phi(p_y; t_i)], \quad (3)$$

where t_i and t_r are the instants of ionization and recollision, respectively. The first term $\tfrac{1}{2}p_y^2(t_r - t_i)$ represents the phase difference between the direct and the rescattered electrons accumulated in the laser field [39]. The second term α is the phase of the scattering amplitude of the target ion, which is determined by the molecular structure [35, 40]. The third term corresponds to the phase induced by the electronic dynamics, where $\phi(0; t_i)$ and $\phi(p_y; t_i)$ are the phases of transverse momentum distribution amplitudes (TMDAs) for the direct and the rescattered electrons at the instant of tunneling [26],

respectively. The TMDA of the superposition state has the form

$$\phi(p_y; t_i) = \arg[c_1 A_1(p_y; t_i) + c_2 A_2(p_y; t_i)e^{-i\theta(t_i)}]. \quad (4)$$

Here $A_{1,2}$ represent the TMDAs for the ground state and the first excited state that compose the superposition state, respectively. $\theta(t_i) = \Delta E t_i + \theta_0$ is the relative phase between the two states.

For the symmetric molecule H_2^+, the first two terms in equation (3) are symmetric about $p_y = 0$. Moreover, the TMDA of the ground state possesses a global phase [26], and thus the third term $\phi(0; t_i) - \phi(p_y; t_i) = 0$ in equation (3). Therefore, the recollision-based holographic pattern determined by equation (3) is symmetric about $p_y = 0$. For the asymmetric molecule HeH^{2+}, the phase of the scattering amplitude, i.e. the second term in equation (3) is asymmetric with respect to $p_y = 0$. As a consequence, these holographic fringes determined by equation (3) is asymmetric, as shown in figure 2(a).

To retrieve the electronic dynamical information encoded in the third term in equation (3), we need to eliminate the first two terms in this equation which are irrelevant to the electron motion. For the symmetric molecule, these two terms are symmetric about $p_y = 0$, and thus can be eliminated by performing the subtraction $\Delta\varphi_+ - \Delta\varphi_- = \phi(-|p_y|) - \phi(|p_y|)$ ($\Delta\varphi_\pm$ represent the holographic interference phase $\Delta\varphi(p_y)$ for $p_y > 0$ and $p_y < 0$ respectively) [26]. When it comes to the asymmetric molecule HeH^{2+}, the second term in equation (3) is asymmetric about $p_y = 0$, so that it can not be eliminated with this subtraction. Here we employ the ground state of HeH^{2+} as a reference, and expose it to the same laser pulse as that for the superposition state (our target). As explained above, the first term in equation (3) is determined by the laser pulse and the second term is determined by the molecular structure, and thus these terms are the same for the ground state and our superposition state ionized by the same laser pulse. Therefore, with this reference, we are able to eliminate the first two terms in equation (3) by performing a subtraction between the interference phase $\Delta\varphi(p_y)$ of our target and that of the reference. Based on this, we can extract the information about the charge migration from the third term in equation (3).

The first step of our procedure is separating the recollision-based holographic fringes from other types of interference patterns in the PEMDs. Here we utilize the Fourier frequency filter method. As shown in figures 3(a)–(c), we perform 2D Fourier transformations of the PEMDs in figures 2(a)–(c). The contributions from different kinds of interferences in the Fourier transformed spectra are separated from each other. The recollision-based holographic interference structures that we concentrate on are identified as the distributions along the f_y axis with near zero f_x, as indicated by the orange ellipses in figures 3(a)–(c). These distributions are enlarged in figures 3(g)–(i) for a better visualization. Then, we select these frequency regions and Fourier transform them back to the momentum space. The results are presented in figures 3(d)–(f), where the near vertical fringes are eliminated
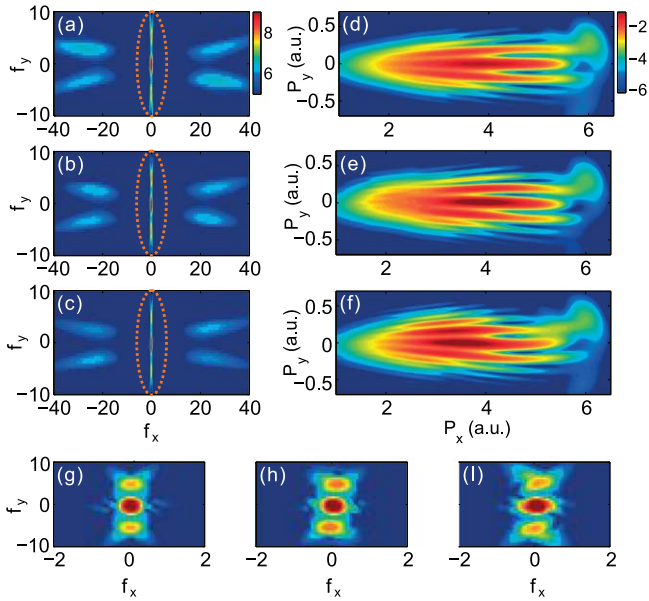
J. Phys. B: At. Mol. Opt. Phys. **51** (2018) 245602

M He *et al*

Figure 3. (a)–(c) Two-dimensional (2D) Fourier transformations of the PEMDs in figures 2(a)–(c), respectively. The orange ellipses indicate the structures correspond to the near-forward SFPH interference. (g)–(I) Zooming of the frequency spectra to highlight the frequency regions marked by the orange ellipses in (a)–(c), respectively. (d)–(f) Fourier transform back the structures indicated by orange ellipses in (a)–(c) to momentum space.

Figure 4. (a) Cuts of the PEMD from figures 3(d) and (e) at longitudinal momentum $p_x = 3.6$ a.u. presented by the purple curve and blue curve, respectively. (b) The recollision-based holographic interference phases $\Delta\varphi_{g-,s-}$ extracted from (a) for the ground state (purple curve) and superposition state (blue curve), respectively. The insert shows the difference between $\Delta\varphi_{g-,s-}$ as a function of transverse momentum p_y.

completely and clear recollision-based holographic fringes are separated successfully.

To demonstrate how to extract electronic dynamics from the recollision-based SFPH patterns, we cut a slice at $p_x = 3.6$ a.u. from the recollision-based holographic fringes in figures 3(d) and (e). The slice from the superposition state (ground state) is presented by the blue curve (purple curve) in figure 4(b). The modulations of these slices correspond to the holographic interference stripes. It is clearly shown that the positions of the minima and maxima of the modulations for the superposition state shift with respect to those for the ground state. From these slices, we extract the holographic interference phases $\Delta\varphi(p_y)$ as functions of the lateral momentum for both the ground state and the superposition state, as shown in figure 4(b). The purple curve represents the interference phase of the ground state ($\Delta\varphi_{g-}$) and the blue curve represents that of the superposition state ($\Delta\varphi_{s-}$) with $p_y < 0$. By performing the subtraction $\Delta\varphi_{g-} - \Delta\varphi_{s-}$, the first two terms in equation (3) are eliminated, and thus we obtain the third term, from which we are able to extract electronic dynamical information. As presented in the insert of figure 4(b), this subtraction $\Delta\varphi_{g-} - \Delta\varphi_{s-}$ is a nearly linear function of lateral momentum $|p_y|$. We mention that in the recent experiment [41], the asymmetric recollision-based holographic interference has been observed. It means that the observation of the asymmetric holographic pattern induced by the electronic dynamics is experimentally accessible, which will encourage the further attempts on extracting interference phase structure with our scheme in experiment.

According to the delay theorem of Fourier transformation $\mathcal{F}[\Psi(y - y_d)] = e^{-iy_d P_y}\mathcal{F}[\Psi(y)]$, when the wave function $\Psi(y)$
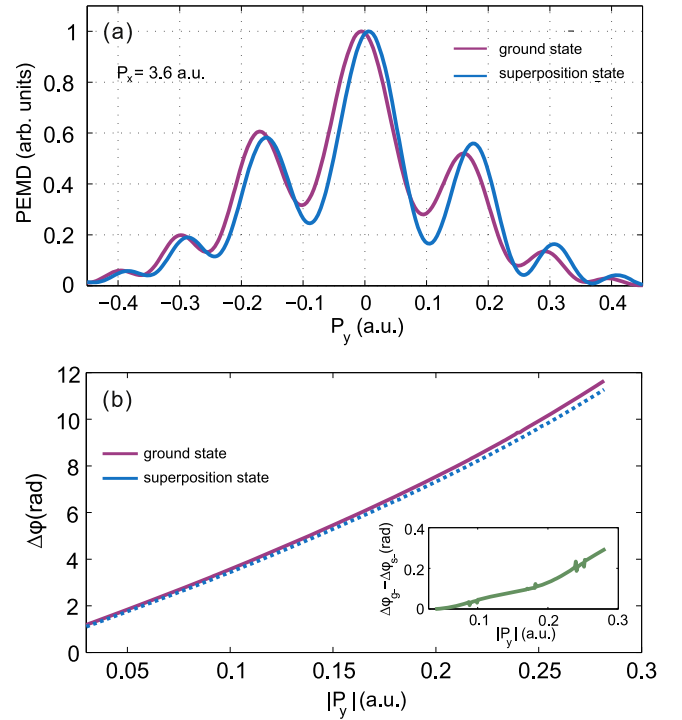
of the superposition state of HeH^{2+} has a shift y_d with respect to that of the ground state in the coordinate space, a linear phase $-y_d p_y$ will be induced in the momentum space [26]. Therefore, the nearly linear phase difference $\Delta\varphi_{g-} - \Delta\varphi_{s-}$ in the momentum distribution indicates the shift y_d between the position of the EWP of the superposition state and that of the ground state in the coordinate space. It means that the slope s of this phase difference explicitly indicates the shift of the transient position of the superposition state with respect to that of the ground state [26], i.e. $y_d = s$.

At the longitudinal momentum $p_x = 3.6$ a.u. the slope of $\Delta\varphi_{g-} - \Delta\varphi_{s-}$ shown in figure 4(b) is $s = 0.83$. Therefore, we obtain the shift $y_d = s = 0.83$ a.u. as we demonstrate above. The tunneling ionization time for $p_x = 3.6$ a.u. can be retrieved by applying the classical relation $p_x = -\frac{1}{2}\int_{t_i}^{\infty} E(t)dt$. Thus, the result above indicates that at this instant the transient position of the EWP of the superposition state has a shift of 0.83 a.u. with respect to that of the ground state.

Then we extract the holographic interference phases and calculate the phase differences $\Delta\varphi_{g-} - \Delta\varphi_{s-}$ at longitudinal momentum p_x ranges from 3 to 4.5 a.u. By performing the linear fitting on these phase differences, we obtain their slopes s. These slopes indicate the shifts ($y_d = s$) of the positions of the EWPs of the superposition state with respect to that of the ground state at different instants. Note that the p_x range (3 to 4.5 a.u.) corresponds to the time interval of 0.8 fs. In figure 5,
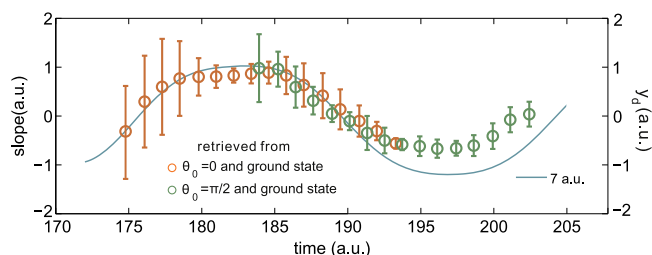
Figure 5. The colored circles represent the slope of the quantity $\Delta\varphi_{g-} - \Delta\varphi_{s-}$ as a function of time. $\Delta\varphi_{g-}$ is extracted from the PEMD of ground state in figure 3(d). $\Delta\varphi_{s-}$ are extracted from the PEMDs in figures 3(e) and (f) for superposition state with initial relative phase $\theta_0 = 0$ (orange circles) and $\pi/2$ (green circles), respectively. The error bars indicate the 95% confidence interval in the slope fitting progress. The solid blue curve is the temporal evolution of the shift of the position for the maximum density of the field-free superposition state of HeH^{2+} (with $c_g^2:c_e^2 = 32:1$) with respect to that of the field-free ground state.

the oscillation of the shift y_d during this interval is shown by the orange circles with error bars. To observe the charge migration during the whole oscillation period, we also employ the recollision-based SFPH pattern in figure 3(f) from the superposition state with initial relative phase $\theta_0 = 0.5\,\pi$. The extracted slopes are indicated by the green circles in figure 5. For comparison, we trace the shift of the position for the maximum density of the field-free superposition state with respect to that of the field-free ground state, as indicated by the blue solid curve in figure 5. The agreement between this shift and the extracted slope s is excellent, it clearly shows that the ultrafast charge migration in HeH^{2+} during the whole oscillation period is visualized successfully with our method. This result demonstrates we can generalize our SFPH based method to investigate the electronic dynamics in asymmetric molecules.

3. Conclusion

In conclusion, we extend our SFPH based scheme [26] to observe the ultrafast charge migration in the asymmetric molecule. We investigate the tunneling ionization of both the coherent superposition state and the ground state of HeH^{2+} by numerically solving TDSE. The Fourier frequency filter method is proposed to separate the recollision-based SFPH pattern from the mixed interference structures in the PEMD, from which we extract the holographic interference phase. By employing the ground state of the asymmetric molecule as a reference, we extract the differential between the holographic interference phase of the superposition state and that of the ground state. This phase difference is a nearly linear function of the lateral momentum, the slope of which indicates the shift of the transient position of the EWP of the superposition state with respect to that of the ground state. Thus the ultrafast charge migration in the asymmetric molecule can be directly visualized. Our work will encourage the investigation of the attosecond electronic dynamics in more complex molecules with SFPH method.

ORCID iDs

Mingrui He ● https://orcid.org/0000-0002-7562-581X

References

[1] Calegari F *et al* 2014 Ultrafast electron dynamics in phenylalanine initiated by attosecond pulses *Science* **346** 6207
[2] Belshaw L, Calegari F, Duffy M, Trabattoni A, Poletto L, Nisoli M and Greenwood J 2012 Observation of ultrafast charge migration in an amino acid *J. Phys. Chem. Lett.* **3** 3751–4
[3] Lünnemann S, Kuleff A and Cederbaum L 2008 Ultrafast charge migration in 2-phenylethyl-N, N-dimethylamine *Chem. Phys. Lett.* **450** 232–5
[4] Yuan K and Bandrauk A 2017 Exploring coherent electron excitation and migration dynamics by electron diffraction with ultrashort x-ray pulses *Phys. Chem. Chem. Phys.* **8** 2229–35
[5] Kuleff A and Cederbaum L 2011 Radiation generated by the ultrafast migration of a positive charge following the ionization of a molecular system *Phys. Rev. Lett.* **106** 053001
[6] Lépine F, Ivanov M and Vrakking M 2014 Attosecond molecular dynamics: fact or fiction? *Nat. Photon.* **8** 195–204
[7] Calegari F, Sansone G, Stagira S, Vozzi G and Nisoli M 2016 Advances in attosecond science *J. Phys. B: At. Mol. Opt. Phys.* **49** 062001
[8] Yuan K and Bandrauk A 2013 Monitoring coherent electron wave packet excitation dynamics by two-color attosecond laser pulses *J. Chem. Phys.* **145** 194304
[9] Breidbach J and Cederbaum L 2005 Universal attosecond response to the removal of an electron *Phys. Rev. Lett.* **94** 033901
[10] Mineo H, Lin S and Fujimura Y 2013 Coherent-electron dynamics of (P)-2, 2-biphenol induced by ultrashort linearly polarized UV pulses: angular momentum and ring current *J. Chem. Phys.* **138** 074304
[11] Mendive-Tapia D, Vacher M, Bearpark M and Robb M 2013 Coupled electron-nuclear dynamics: charge migration and charge transfer initiated near a conical intersection *J. Chem. Phys.* **139** 044110
[12] Remacle F and Levine R 2006 An electronic time scale in chemistry *Proc. Natl Acad. Sci.* **103** 6793
[13] Gaumnitz T *et al* 2017 Streaking of 43-attosecond soft-x-ray pulses generated by a passively CEP-stable mid-infrared driver *Opt. Express* **25** 27506–18
[14] Huismans Y *et al* 2011 Time-resolved holography with photoelectrons *Science* **331** 61
[15] Wang D *et al* 2018 Momentum gate for tunneling electrons with a circularly polarized control field *Phys. Rev. A* **98** 053410

[16] Li L *et al* 2018 Real-time observation of molecular spinning with angular high-harmonic spectroscopy *Phys. Rev. Lett.* **121** 163201

[17] Chen Y, Zhou Y, Li Y, Li M, Lan P and Lu P 2018 Rabi oscillation in few-photon double ionization through doubly excited states *Phys. Rev.* A **97** 013428

[18] Goulielmakis E *et al* 2010 Real-time observation of valence electron motion *Nature* **466** 739–43

[19] Ott C *et al* 2014 Reconstruction and control of a time-dependent two-electron wave packet *Nature* **516** 374–8

[20] Niikura H, Villeneuve D and Corkum P 2005 Mapping attosecond electron wave packet motion *Phys. Rev. Lett.* **94** 083003

[21] Chelkowski S, Bredtmann T and Bandrauk A 2012 High-order-harmonic generation from coherent electron wave packets in atoms and molecules as a tool for monitoring attosecond electrons *Phys. Rev.* A **85** 033404

[22] Kraus P *et al* 2015 Measurement and laser control of attosecond charge migration in ionized iodoacetylene *Science* **350** 790–5

[23] Ossiander M *et al* 2017 Attosecond correlation dynamics *Nat. Phys.* **13** 280–5

[24] Walt S, Ram N, Atala M, Shvetsov-Shilovski N, von Conta A, Baykusheva D, Lein M and Wörner H 2017 Dynamics of valence-shell electrons and nuclei probed by strong-field holography and rescattering *Nat. Commun.* **8** 15651

[25] Haertelt M, Bian X, Spanner M, Staudte A and Corkum P 2016 Probing molecular dynamics by laser-induced backscattering holography *Phys. Rev. Lett.* **116** 133001

[26] He M, Li Y, Zhou Y, Li M, Cao W and Lu P 2018 Direct visualization of valence electron motion using strong-field photoelectron holography *Phys. Rev. Lett.* **120** 133204

[27] Shvetsov-Shilovski N and Lein M 2018 Effects of the Coulomb potential in interference patterns of strong-field holography with photoelectrons *Phys. Rev.* A **97** 013411

[28] Song X *et al* 2017 Attosecond interference induced by Coulomb-field-driven transverse backward-scattering electron wave-packets *Phys. Rev.* A **95** 033426

[29] Lindner F *et al* 2005 Attosecond double-slit experiment *Phys. Rev. Lett.* **95** 040401

[30] Arbó D, Ishikawa K, Schiessl K, Persson E and Burgdörfer J 2010 Intracycle and intercycle interferences in above-threshold ionization: the time grating *Phys. Rev.* A **81** 021403(R)

[31] Tan J, Li Y, Zhou Y, He H, Chen Y, Li M and Lu P 2018 Identifying the contributions of multiple-returning recollision orbits in strong-field above-threshold ionization *Opt. Quant. Electron.* **50** 57

[32] He M, Zhou Y, Li Y, Li M and Lu P 2016 Temporal and spatial manipulation of the recollision wave packet in strong-field photoelectron holography *Phys. Rev.* A **93** 033406

[33] Xie X 2015 Two-dimensional attosecond electron wave-packet interferometry *Phys. Rev. Lett.* **114** 173003

[34] Richter M, Kunitski M, Schöffler M, Jahnke T, Schmidt L, Li M, Liu Y and Dörner R 2015 Streaking temporal double-slit interference by an orthogonal two-color laser field *Phys. Rev. Lett.* **114** 143001

[35] Zhou Y, Tolstikhin O and Morishita T 2016 Near-forward rescattering photoelectron holography instrong-field ionization: extraction of the phase of the scattering amplitude *Phys. Rev. Lett.* **116** 173001

[36] Tong X, Watahiki S, Hino K and Toshima N 2007 Numerical observation of the rescattering wave packet in laser-atom interactions *Phys. Rev. Lett.* **99** 093001

[37] Bian X and Bandrauk A 2012 Orientation dependence of nonadiabatic molecular high-order-harmonic generation from resonant polar molecules *Phys. Rev.* A **86** 053417

[38] Bian X and Bandrauk A 2014 Orientation-dependent forward-backward photoelectron holography from asymmetric molecules *Phys. Rev.* A **89** 033423

[39] Bian X and Bandrauk A 2012 Attosecond time-resolved imaging of molecular structure by photoelectron holography *Phys. Rev. Lett.* **108** 263003

[40] He M, Zhou Y, Li Y, Li M and Lu P 2017 Revealing the target structure information encoded in strong-field photoelectron hologram *Opt. Quant. Electron.* **49** 232

[41] Meckel M *et al* 2014 Signatures of the continuum electron phase in molecular strong-field photoelectron holography *Nat. Phys.* **10** 594

[42] Ke S, Zhao D, Liu Q and Liu W 2018 Adiabatic transfer of surface plasmons in non-Hermitian graphene waveguides *Opt. Quant. Elecron.* **50** 393

[43] Ma X, Zhou Y, Li N, Li M and Lu P 2018 Attosecond control of correlated electron dynamics in strong-field nonsequential double ionization by parallel two-color pulses *Opt. Laser Technol.* **108** 235–240

[44] Liu Q, Ke S and Liu W 2018 Mode conversion and absorption in an optical waveguide under cascaded complex modulations *Opt. Quant. Electron.* **50** 356